2004

Vertical Dynamical Transport of Mesospheric Constituents by Dissipating Gravity Waves

Alan Z. Liu
Embry Riddle Aeronautical University - Daytona Beach, liuz2@erau.edu

Chester S. Gardner
University of Illinois at Urbana-Champaign

ELSEVIER

Journal of Atmospheric and Solar-Terrestrial Physics 66 (2004) 267–275

Journal of ATMOSPHERIC AND SOLAR-TERRESTRIAL PHYSICS

www.elsevier.com/locate/jastp

Vertical dynamical transport of mesospheric constituents by dissipating gravity waves

Alan Z. Liu*, Chester S. Gardner

Electro-Opt Lab, 308 CSRL, MC229, Departments of Electrical and Computer Engineering, University of Illinois at Urbana-Champaign 1308, West Main Street, Urbana, IL 61801, USA

Received 13 January 2003; received in revised form 29 September 2003; accepted 6 November 2003

Abstract

Over 400 h of Na wind/temperature lidar observations, obtained at the Starfire Optical Range, NM, are used to study the vertical dynamical transport of Na in the mesopause region between 85 and 100 km. Dynamical transport occurs when dissipating, non-breaking gravity waves impart a net vertical displacement in atmospheric constituents as they propagate through a region. We show that the vertical constituent flux can be related in a simple way to the vertical heat flux. Breaking gravity waves also contribute to eddy transport by generating turbulence. Because eddy transport is a mixing process, it only occurs in the presence of a gradient in the concentration profile of the constituent, while dynamical transport can be sustained even in the absence of such a gradient. The dynamical Na flux is compared with the predicted eddy flux. The maximum downward dynamical flux of Na is -280 m/s cm^3 at 88 km. The maximum downward eddy flux is -160 m/s cm^3 at the same altitude assuming the diffusion coefficient is 200 m^2/s. The observational results are consistent with theoretical predictions below 93 km and show that dynamical transport often exceeds the vertical transport associated with eddy diffusion. The theoretical models are used to predict the dynamical and eddy fluxes of atomic oxygen and show that for this constituent, dynamical transport is also a significant transport mechanism.

Keywords: Na flux; Gravity waves; Na lidar; Wave dissipation; Eddy diffusion

1. Introduction

Eddy transport by turbulent mixing is thought to play an important role in establishing the constituent structure of the middle atmosphere below the turbopause. Eddy mixing, which is similar to diffusion, transports constituents from regions of higher concentrations to those with lower concentrations. Gravity waves contribute to this transport process by generating turbulence when they break. Considerable theoretical and experimental work has been directed at establishing the relationships between gravity wave dissipation mechanisms and the turbulence characteristics. Early work focused on identifying the instability mechanisms which lead to wave breaking (e.g. Hodges, 1967; Lindzen, 1981) and assessing the resulting effects on momentum transport and mean flow modification. This research clearly demonstrated that the turbulent drag contributed by breaking gravity waves has a profound affect on global circulation, especially in the middle atmosphere. It is responsible for the deceleration of mean zonal wind in the upper mesosphere and the cold summer mesopause. Weinstock (1984) showed that nonlinear interactions of non-breaking gravity waves can also contribute to eddy mixing. Radar and in situ rocket observations have provided direct measurements of middle atmosphere turbulence as well as estimates of the associated eddy diffusion coefficient (e.g. Lübken et al., 1993, 1994; Lübken, 1997; Hocking, 1986; Watkins et al., 1988; Thrane et al., 1987).

It is well known that dissipating gravity waves play an important role in the vertical transport of heat and momentum (Walterscheid, 2001). Numerous papers have reported theoretical calculations and observational data which have

* Corresponding author. Tel.: +1-217-333-6982; fax: +1-217-333-4303.

E-mail address: liuzr@uiuc.edu (A.Z. Liu).

1364-6826/$ - see front matter © 2004 Elsevier Ltd. All rights reserved.
doi:10.1016/j.jastp.2003.11.002

quantified the vertical fluxes of heat and horizontal momentum in the middle atmosphere (e.g. Reid and Vincent, 1987; Tao and Gardner, 1995; Gardner et al., 1998, 1999; Fritts and van Zandt, 1993; Tsuda et al., 1990). Constituent transport by non-breaking waves has received far less attention. Dynamical transport arises when the dissipating waves impart a net vertical displacement in the atmospheric constituent as they propagate through a region. It is fundamentally different than the eddy mixing or diffusion process associated with the turbulence generated by breaking waves. The Stokes drift studied by Walterscheid and Hocking (1991) and Hocking and Walterscheid (1993) is an example of a wave-induced displacement mechanism that contributes to dynamical transport. Walterscheid (1981) and Weinstock (1984) derived the relationship between the effective vertical diffusivity and the vertical heat flux. More recently Walterscheid et al. (1987) and Walterscheid and Schubert (1989) showed that the combined effects of chemistry and wave perturbations could also contribute to an effective vertical constituent flux. Although the importance of dynamical transport has been established by this theoretical work, most numerical models of middle atmosphere composition and structure only incorporate eddy transport to predict the constituent profiles. Because of the difficulties in measuring simultaneously, the vertical wind and constituent number density perturbations in the middle atmosphere, no direct measurements of dynamical constituent fluxes in this region have been reported until now.

In this paper, we discuss the relative importance of eddy and dynamical transport processes and show that the vertical constituent flux can be related in a simple way to the vertical heat flux. We then use high resolution Na wind/temperature lidar data collected at the starfire optical range (SOR), New Mexico to measure the vertical Na flux profile. The results are compared with theoretical predictions of both the eddy and dynamical fluxes. The results are then used to predict the dynamical flux of atomic oxygen in the upper mesosphere and lower thermosphere. We include a detailed analysis of the constituent flux measurement errors to help guide the design of future observational campaigns.

2. Vertical constituent flux associated with eddy transport

Above the turbopause ($\sim$ 120 km) the earth's atmosphere is mixed by molecular diffusion. In the middle atmosphere, below the turbopause, eddy diffusion is the dominant mixing process. When there exists a vertical gradient in the concentration profile of a constituent, the combined effects of the gradient and eddy mixing leads to a net transport of the constituent from regions of higher concentrations to those with lower concentrations. Eddy transport weakens the gradient and drives the constituent distribution towards homogeneity.

By assuming that eddy diffusion is a larger scale analog of molecular diffusion, the mixing process and its effects on the constituent distribution can be characterized in terms of an eddy diffusion coefficient. The vertical eddy flux (EF) is calculated using the continuity equation and is given by the well-known expression (Colegrove et al., 1966)

$$EF = -D_{zz}\bar{\rho}_a(z)\frac{d}{dz}\frac{\bar{\rho}(z)}{\bar{\rho}_a(z)} = -D_{zz}\bar{\rho}(z) \times \left(\frac{1}{H} - \frac{1}{H_\rho(z)} + \frac{d\ln T}{dz}\right), \quad (1)$$

where $\bar{\rho}(z)$ and $\bar{\rho}_a(z)$ are the unperturbed constituent and atmospheric number density profiles (overbar denotes time average) in $1/cm^3$, respectively; D_{zz} is the vertical eddy diffusion coefficient in m^2/s; T is the temperature profile in K, H is the atmospheric scale height in m, and

$$H_\rho(z) = -\left[\frac{d\ln\bar{\rho}(z)}{dz}\right]^{-1} \quad (2)$$

is the constituent scale height in m. EF is in unit of $m/s/cm^3$. For an isothermal atmosphere, Eq. (1) becomes

$$EF = -D_{zz}\bar{\rho}(z)\left[\frac{1}{H} - \frac{1}{H_\rho(z)}\right]. \quad (3)$$

In an isothermal atmosphere, the eddy flux is downward whenever the constituent scale height H_ρ is less than H and upward whenever $H_\rho > H$. The eddy flux is zero when $H_\rho = H$, i.e. the gradient of constituent concentration profile $\bar{\rho}(z)/\bar{\rho}_a(z)$ is zero (see Eq. (1)).

To determine the eddy flux of a constituent, the diffusion coefficient, D_{zz}, and the concentration profile, $\bar{\rho}(z)/\bar{\rho}_a(z)$, must be known. Initial research on eddy diffusion focused on deriving an effective diffusion coefficient to account for constituent transport by solving the continuity equation (e.g., Colegrove et al., 1966). As various theories and models of dissipating gravity waves were developed, it was recognized that these waves could also play an important role in constituent transport by generating turbulence. In the linear theory of wave dissipation, a wave-induced instability is the source of the turbulent diffusion (e.g., Hodges, 1967; Lindzen, 1981), while in non-linear theory, eddy diffusion is caused by non-linear wave–wave interactions (Weinstock, 1984).

3. Vertical constituent flux associated with dynamical transport

In addition to transporting heat and momentum, gravity waves also transport atmospheric constituents. Vertical dynamical transport by dissipating waves is fundamentally different than transport by eddy diffusion. Eddy transport is a mixing process while dynamical transport arises when the dissipating waves impart a net vertical displacement in the atmospheric constituent as they propagate through a region.

Waves can contribute to eddy transport by generating turbulence when they break. Dynamical transport is associated with propagating (non-breaking) waves. One such example is the Stokes drift studied by Walterscheid and Hocking (1991) and Hocking and Walterscheid (1993).

The vertical flux associated with the dynamical transport of a constituent is just the expectation of the product of the wave-induced perturbations in vertical velocity (w') and constituent number density (ρ'), viz. $\langle w'\rho'\rangle$ (angle brackets denote ensemble average). When chemical effects can be ignored, the constituent number density perturbations associated with gravity waves can be expressed in terms of the concomitant temperature perturbations (T') (Senft and Gardner, 1991; Bills and Gardner, 1993),

$$\rho(z) = \bar{\rho}(z + (\Gamma_e - \Gamma_a)^{-1}T')\exp\left(\frac{1}{\gamma - 1}\frac{T'}{\bar{T}}\right), \tag{4}$$

where $\gamma = 1.4$ is the ratio of specific heats and $\bar{T}$ is the unperturbed temperature, $\Gamma_e = -d\bar{T}/dz$ is the environment temperature lapse rate and Γ_a is the dry adiabatic lapse rate. For sufficiently small temperature fluctuations, the constituent fluctuations can be approximated by the first-order term of the perturbation series expansion of Eq. (4) about T'.

$$\frac{\rho'}{\bar{\rho}} \approx \frac{1}{\gamma - 1}\left(1 - \frac{\gamma - 1}{\Gamma_a - \Gamma_e}\frac{\bar{T}}{H_\rho}\right)\frac{T'}{\bar{T}} = \frac{1}{\gamma - 1}\left(1 - \frac{\gamma}{1 - \Gamma_e/\Gamma_a}\frac{H}{H_\rho}\right)\frac{T'}{\bar{T}}. \tag{5}$$

Thus, the vertical dynamical flux (DF) of the constituent is approximately proportional to the vertical heat flux

$$DF = \langle w'\rho'\rangle \approx \frac{1}{\gamma - 1}\frac{\bar{\rho}}{\bar{T}} \times \left(1 - \frac{\gamma}{1 - \Gamma_e/\Gamma_a}\frac{H}{H_\rho}\right)\langle w'T'\rangle. \tag{6}$$

In the absence of wave dissipation, the wave perturbations in temperature are proportional to vertical displacement so that w' and T' are nearly orthogonal, and the vertical heat and constituent fluxes are near zero. Wave dissipation mechanisms such as saturation, diffusive damping, critical layer interactions, and instabilities alter the phase relationship between w' and T', thus giving rise to a net heat and constituent transport. Unlike eddy flux, which requires a concentration gradient to sustain the vertical transport (mixing) process (see Eq. (1)), the dynamical flux can be non-zero even if the concentration gradient is zero (DF is non-zero when $H_\rho = H$ in Eq. (6)).

Several authors have explored the relationship between wave-induced diffusivity and the vertical heat flux. Walterscheid (1981) and later Weinstock (1984) used the thermodynamic equation to show that the effective vertical diffusivity can also be expressed in terms of the vertical heat flux, Γ_a and Γ_e, and the mean square lapse rate perturbations $\langle(\partial T'/\partial z)^2\rangle$ as

$$D_{zz} = -(\Gamma_a - \Gamma_e)\frac{\langle w'T'\rangle}{\langle(\partial T'/\partial z)^2\rangle}. \tag{7}$$

By combining Eqs. (3), (6), and (7), the dynamical flux can be expressed in terms of the eddy flux.

$$DF = \langle w'\rho'\rangle \approx \frac{\gamma H/(1 - \Gamma_e/\Gamma_a) - H_\rho}{1 - H_\rho/H} \times \frac{\langle(\partial T'/\partial z)^2\rangle}{(\Gamma_a - \Gamma_e)(\gamma - 1)\bar{T}}\,EF. \tag{8}$$

At mesopause heights where the mean square lapse rate is 50–100 K^2/km^2, the dynamical flux is comparable to the eddy flux. It could exceed the eddy flux significantly, when the constituent scale height is close to H. Thus, the vertical dynamical transport of minor constituents by dissipating gravity waves is expected to be significant and at least as important as eddy transport.

It is important to keep in mind that Eqs. (4), (5), and (8) are approximate formulas that were derived by ignoring chemistry and nonlinear perturbation effects. In the real atmosphere for many constituents, the chemical reaction times are short compared to the gravity wave periods and so chemistry can have a significant influence on the wave-induced perturbations of constituent densities (Walterscheid and Schubert, 1989). When the constituent scale height is small, nonlinear effects can be important so that the first-order perturbation term may not be sufficient to characterize the constituent fluctuations (Gardner and Shelton, 1985).

4. Computing the vertical constituent flux from observations

The observed gravity wave perturbations in temperature and winds are the sum of the contributions from many different waves propagating in different directions that were generated by different sources (primarily in the lower atmosphere). According to the Central Limit Theorem, when the number of independent waves becomes sufficiently large, the temperature and vertical wind perturbations (T' and w') can be modeled as zero-mean Gaussian-distributed random processes. Because the constituent fluctuations are approximately proportional to the temperature fluctuations, ρ' is also approximately Gaussian distributed. For the Na lidar measurements reported here, the dominant error source is photon noise, which is Poisson distributed. To achieve measurement accuracies of a few K, a few m/s, and a few tenths percent in Na number density, signal levels exceeding a few tens of thousands of photon counts per resolution cell are required (Papen et al., 1995). At these high signal levels, the Central Limit Theorem predicts that the instrument measurement errors ($\Delta T, \Delta w$ and $\Delta\rho$) are also zero-mean Gaussian-distributed random processes.

Gardner and Yang (1998) analyzed the statistics of the vertical wind and temperature perturbations measured at SOR and confirmed the Gaussian hypothesis. The statistics of the Na number density fluctuations are examined in the appendix. Because of nonlinear effects, Eq. (5) is only an approximate and as a consequence the Na statistics depart somewhat from the Gaussian model. In fact, the fluctuations are approximately log-normal. However, when the fluctuations are small the Gaussian model is a valid approximation and is used in the following to characterize the errors in the measured Na fluxes.

When measuring constituent fluxes, we are actually measuring the cross correlation between the vertical wind and constituent number density perturbations. Since the constituent fluctuations are approximately proportional to the temperature fluctuations, constituent fluxes are related to the vertical wind and temperature correlations, which are small (Gardner and Yang, 1998; Gardner et al., 2002). Because the constituent flux is small compared to the variance of an instantaneous, point flux measurement, long averaging times are required to obtain statistically significant flux estimates. To obtain useful flux measurements, vertical and temporal resolution must be sufficient to observe the important short vertical scale, high-frequency waves. At mesopause heights, gravity waves have vertical wavelengths as short as 1 km and intrinsic periods as short as 5 min. The required long averaging times, high resolution, and high accuracy of the vertical wind and constituent measurements, present considerable observational challenges for measuring scientifically useful constituent fluxes.

Na fluxes can be measured by pointing the lidar at zenith to observe w and ρ_{Na} directly. Dual-beam off-zenith observations can also be used to compute heat and constituent fluxes by employing an analysis similar to that used to compute momentum fluxes (Kudeki and Franke, 1998). The analysis of the Na flux errors for zenith measurements is nearly identical to that employed by Gardner and Yang (1998) to characterize the heat flux errors. We assume the vertical wind and Na number density fluctuations are approximately Gaussian distributed. For our lidar data, there is a small, negligible correlation between the wind and Na number density errors (resulting Na flux bias $< 10^{-3}$ m/s/cm^3). The instantaneous, point estimate of the dynamical flux (DF), its mean and variance are

$$DF = (w' + \Delta w)(\rho'_{\mathrm{Na}} + \Delta\rho_{\mathrm{Na}}), \tag{9}$$

$$\langle DF\rangle = \langle w'\rho'_{\mathrm{Na}}\rangle, \tag{10}$$

$$\mathrm{var}(DF) = \langle w'\rho'_{\mathrm{Na}}\rangle^2 + [\langle (w')^2\rangle + \langle (\Delta w)^2\rangle] \times [\langle (\rho'_{\mathrm{Na}})^2\rangle + \langle (\Delta\rho_{\mathrm{Na}})^2\rangle]. \tag{11}$$

The magnitude of the dynamical Na flux is typically less than a few hundred m/s cm^3 while the standard deviation of the instantaneous, point flux estimate can exceed 1000 m/s cm^3 even in the absence of instrument errors. To reduce this variance, the flux estimates are averaged over time or altitude or both

$$\overline{DF} = \frac{1}{\tau L}\int_{z_0-L/2}^{z_0+L/2} \mathrm{d}z \int_{t_0-\tau/2}^{t_0+\tau/2} \mathrm{d}t (w' + \Delta w) \times (\rho'_{\mathrm{Na}} + \Delta\rho_{\mathrm{Na}}), \tag{12}$$

where τ and L are respectively, the averaging period and height range (overbar denotes sample average). $\overline{DF}$ is an unbiased estimator of $\langle w'\rho'_{\mathrm{Na}}\rangle$, and its variance is

$$\mathrm{var}(\overline{DF}) \approx \frac{\Delta z_{DF}}{L}\,\frac{\Delta t_{DF}}{\tau}[\langle (w')^2\rangle + \langle (\Delta w)^2\rangle] \times [\langle (\rho'_{\mathrm{Na}})^2\rangle + \langle (\Delta\rho_{\mathrm{Na}})^2\rangle], \tag{13}$$

where $\Delta t_{DF} \approx 10$ min and $\Delta z_{DF} \approx 1$ km are the correlation time and correlation length of the dynamical flux estimate. The values of these parameters can be inferred from the data (see appendix in Gardner and Yang, 1998). Note that in this formula, L and τ can never be less than Δz_{DF} and Δt_{DF}, respectively. If the flux estimate is only averaged over time so that $L = \Delta z_{DF}$ and we assume $\tau = 8$ h and use (2.5 m/s)^2 and (500/cm^3)^2 for the total wind and Na number density variances (gravity wave perturbations plus instrument noise), the standard deviation of the time averaged Na flux is 180 m/s/cm^3. Because this value is comparable to the maximum observed Na fluxes, the data must be averaged in altitude and/or over several observation periods to obtain statistically significant flux estimates. The variance given by Eq. (13) arises from the fundamental statistical fluctuations in the flux estimate and is significant even in the absence of instrument errors. We refer to this variance term as the statistical error to distinguish it from other error sources. It is the dominant error source for the SOR Na flux measurements.

For the data reported here, the vertical wind, temperature and Na number density perturbations for each night are calculated by subtracting the time mean from the observations at each altitude for the night and then subtracting the vertical mean in each profile. Thus, the flux involves waves with time scales less than about 8–10 h and vertical scale less than ~15 km. Errors in the sample means ($\Delta\bar{w}$ and $\Delta\bar{\rho}_{\mathrm{Na}}$) can introduce biases into the Na flux measurements. The mean bias error is zero and the variance is (see Gardner and Yang (1998) for the derivation)

$$\mathrm{var}\left(\frac{1}{L}\int_{-L}^{L}\Delta\bar{w}\Delta\overline{\rho'_{\mathrm{Na}}}\mathrm{d}z\right) \approx \frac{\Delta z_{DF}\Delta t_{\mathrm{w}}\Delta t_{\mathrm{Na}}}{L\tau^2}[\langle (w')^2\rangle + \langle (\Delta w)^2\rangle] \times [\langle (\rho'_{\mathrm{Na}})^2\rangle + \langle (\Delta\rho_{\mathrm{Na}})^2\rangle], \tag{14}$$

where $\Delta t_{\mathrm{w}} = \Delta t_{DF} \approx 10$ min and $\Delta t_{\mathrm{Na}} \approx 60$ min are the correlation times for the vertical wind and Na fluctuations. For an 8 h observing period with $L = \Delta z_{DF}$, Eq. (14)

predicts a bias error of 64 m/s/cm^3. Because this variance is inversely proportional to the square of the averaging period τ, it decreases quickly as the averaging period increases.

5. Na flux observations

SOR is located on the Kirtland AFB (35°N, 106.5°W), near Albuquerque, NM. The facility is operated by the Air Force Research Laboratory, Directed Energy Directorate and includes a 3.5-m-diameter steerable telescope. The University of Illinois Na wind/temperature lidar was interfaced with the telescope and used to make nighttime observations of temperature, Na number density, and all three wind components between about 80 and 105 km altitude. A total of over 410 h of measurements were conducted on 60 different nights from June 1998 to November 2000. The lidar and telescope were pointed sequentially at zenith (Z) and 10° off zenith to the north (N), south (S), east (E), and west (W) in the sequence NEZSWZ. Although telescope pointing was calibrated to arcsecond (μrad) accuracy using known star positions, the absolute pointing accuracy of the system was limited by the 1 mrad field of view of the lidar. The error in vertical wind measurements due to this pointing uncertainty is negligible (Gardner and Yang, 1998). At each beam position backscatter profiles of Na number density, radial winds, and temperature were accumulated for approximately 1.5 min before moving to the next position. Approximately 20 s was required to reposition the telescope. The raw wind, temperature, and Na number density data were derived at a spatial resolution of 96 m and were then binned to 1 km to further reduce the uncertainty due to photon noise. At this resolution the mean rms temperature, radial wind, and relative Na number density errors are about ±1.3 K, ±1 m/s, and ±0.4%, respectively, between 92 ± 7.5 km. The resulting Na, temperature, and wind data include gravity wave perturbations with vertical wavelengths larger than 2 km and observed periods longer than 6 min. Details of the experimental setup, data processing, and validation can be found in Gardner and Yang (1998) and Gardner et al. (1998).

Several experiments were conducted during this period to validate the absolute accuracy of the Na lidar wind measurements. Grime et al. (2000) compared radial winds derived by probing persistent meteor trails observed during the 1998 Leonid meteor shower. The Doppler radial wind velocities measured by the lidar agreed with those computed from the rate of change of the meteor trail ranges, within the several m/s error limits of the two measurement techniques. This is the most direct and accurate comparison that can be made since both techniques measure the velocities at the same point. The meteor trails were entrained in the atmosphere so measuring their advection provides a precise unbiased estimate of radial velocity. Larsen et al. (2003) compared the zonal and meridional wind profiles measured by the lidar over White Sands Missile Range (WSMR) 150 km south of SOR, with those inferred from TMA trails released by a rocket payload launched from WSMR during the TOMEX (Turbulent Oxygen Mixing Experiment) campaign. Excellent agreement was obtained between 85 and 105 km altitude, within the ±10 m/s experimental errors of the two techniques. Liu et al. (2002) compared the hourly mean zonal and meridional wind profiles measured by a meteor radar and the Na lidar at SOR and found excellent agreement (correlation coefficients 0.84–0.95) in the composite tidal winds derived from the two datasets around 86 and 93 km. When these two instruments were installed in Maui, Hawaii in 2002 where the meteor detection rate was significantly higher than at SOR, the correlation coefficients between the hourly mean meteor radar and Na lidar winds on individual nights also exceeded 0.9 (Franke et al., 2004). Although these experiments demonstrate clearly the m/s absolute accuracy of the Na lidar wind observations, the Na flux and heat flux measurements reported here, were derived using the vertical wind perturbations computed by subtracting the average wind between 85 and 100 km for each 1.5 min profile. This eliminates any small wind biases that might be introduced by undetected fluctuations in the laser frequency.

We use the SOR Na and vertical wind data to compute the mean vertical Na flux $\langle w'\rho'_{\mathrm{Na}}\rangle$. Only the data from the zenith beams were used to derive the flux profiles. Long averaging periods are required to obtain statistically significant Na flux profiles for the very same reasons extensive averaging is needed for the heat and momentum flux measurements. The mean Na flux for every night was first calculated and then the nightly mean profiles were averaged for all nights. The final profile was smoothed by a 4 km full width Hamming window. The result is shown in Fig. 1 as thick solid line. The dynamical transport is downward throughout the Na layer with a peak value of −280 m/s/cm^3 at 88 km.

Also plotted in Fig. 1 for comparison is the eddy flux predicted by Eq. (1). The eddy flux was calculated from Eq. (1) using the average observed Na number density profile $\bar{\rho}_{\mathrm{Na}}$ and temperature. We used an effective diffusivity of $D_{zz} = 200$ m^2/s, which is typical for this region. In a simulation of gravity wave effects, Mengel et al. (1995) used a value of 130 m^2/s at 80 km in their model and produced reasonable results. Hocking (1990) predicted a value of 200–300 m^2/s. The measured dynamical flux is larger than the eddy flux on the bottom side of the Na layer. An effective vertical diffusivity of about 440 m^2/s would be required to model the total Na flux as an eddy diffusion process at this altitude, which is much larger than the eddy diffusion alone.

The predicted dynamical flux is also shown in Fig. 1. It was computed from Eq. (6) using the averaged Na number density, temperature and the heat flux measured at SOR. The heat flux profile is shown in Fig. 2. The heat flux is downward with a peak value of −2.3 K m/s at about 88 km. There is little heat flux above 95 km because the atmosphere is statically stable in this region and the wave dissipation is negligible (Gardner et al., 2002). Below 92 km the predicted

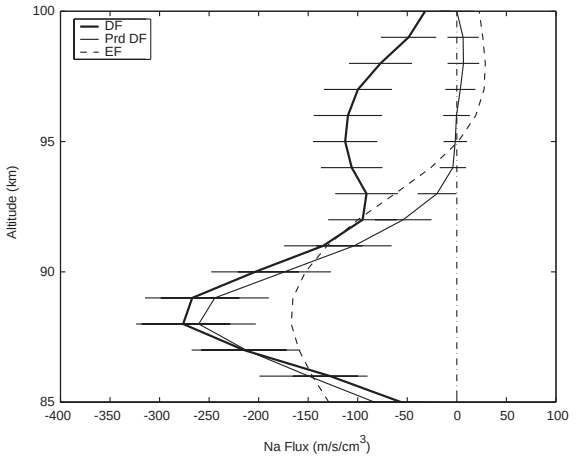

Fig. 1. Observed dynamical flux (thick solid line), predicted dynamical flux (thin solid line) and eddy flux (dashed line) based on all SOR data . The eddy flux is calculated using Eq. (1) with $D_{zz} = 200$ m^2/s. Uncertainties of dynamical fluxes are also shown with error bars of $1-\sigma$.

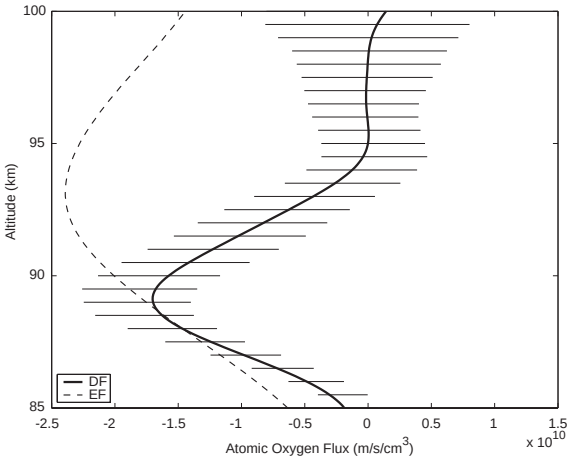

Fig. 3. Predicted dynamical (solid line) and eddy (dashed line) fluxes of atomic oxygen using Eqs. (6) and (1) with $D_{zz}=200$ m^2/s and the calculated heat flux shown in Fig. 2. Uncertainty of the dynamical flux is shown with $1-\sigma$ error bars.

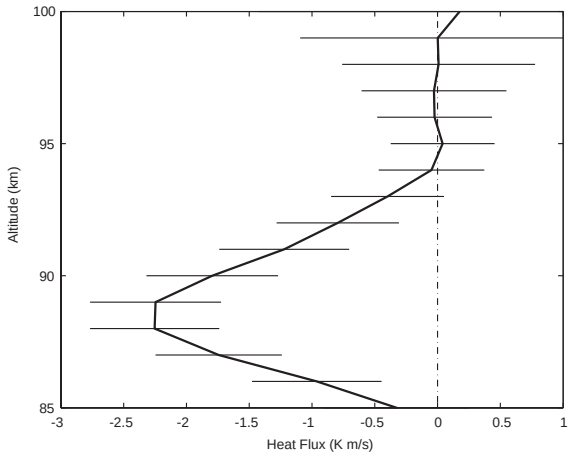

Fig. 2. Heat flux calculated based on all SOR data. Uncertainty of the heat flux is also shown with error bars of $1-\sigma$.

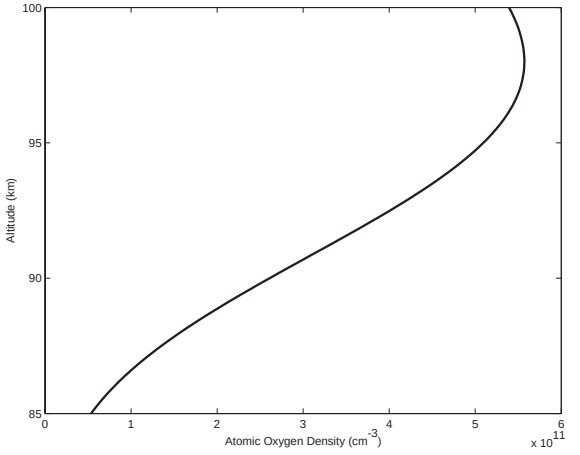

Fig. 4. The atomic oxygen profile from MSIS-00 model, used in calculating dynamical and eddy fluxes shown in Fig. 3.

and measured Na fluxes agree quite well. Above 92 km, the measured dynamical flux is larger than that predicted by Eq. (6). This discrepancy may be related to the chemical reactions on the topside of the Na layer (Plane et al., 1999).

6. Predicted dynamical flux of atomic oxygen

The Na flux results are significant because all atmospheric constituents are affected by dynamical transport associated with dissipating gravity waves. Studies of the Na flux can lead to a better understanding of the impact of dynamical transport on more important mesospheric constituents such as the chemically active odd-oxygen and odd-hydrogen species. For example by measuring the heat flux, the dynamical flux of the atomic oxygen O can be predicted using Eq. (6) with the Na profile parameters replaced by those of the atomic oxygen profile. The predicted dynamical and eddy fluxes of O are plotted in Fig. 3 using a MSIS-00 atomic oxygen profile shown in Fig. 4, and the measured heat flux profile shown in Fig. 2. Just as we saw with Na, the dynamical O flux is significant, with peak value comparable to the eddy flux at $\sim$ 89 km. Obviously, the dynamical flux can have a significant influence on the distribution and vertical transport of atomic oxygen, especially in the region

between 85 and 93 km, where strong wave dissipation occurs (Gardner et al., 2002).

When the heat budget of the middle atmosphere is calculated, it is important to correctly account for the transport of long-lived species such as atomic oxygen. The lifetime of atomic oxygen is about several days above 90 km altitude (Garcia and Solomon, 1985). Atomic oxygen plays an important role in the thermal balance of the middle atmosphere because it absorbs solar UV radiation and releases energy through exothermic chemical reactions such as $O+O+M \rightarrow O_2 + M$ and $O + O_3 \rightarrow O_2 + O_2$ (Mlynczak and Solomon, 1993; Riese et al., 1994). When atomic oxygen is transported below 60 km, it can combine with molecular oxygen generating ozone ($O + O_2 \rightarrow O_3$), which is one of the most important absorbers of solar energy in the middle atmosphere. Thus, atomic oxygen transport is also an important energy transport mechanism. Our results suggest that dynamical transport of constituents such as O may be as significant as the eddy transport in the mesopause region. This has also been demonstrated in model simulations by Hickey et al. (2000), who showed that the gravity wave transport caused a secular variation in O density and moved the O layer downward. Its effect can be greater than eddy diffusion.

7. Conclusions

It has long been assumed that dissipating gravity waves play an important role in constituent transport by generating turbulence when they break. The resulting eddy mixing transports constituents from regions of high concentrations to regions of lower concentrations. In most chemical models, eddy transport is considered to be the main transport effect associated with gravity waves in the middle atmosphere (e.g., Fritts and Dunkerton, 1985). Dynamical transport occurs when dissipating (non-breaking) gravity waves impart a net vertical displacement in the constituent when they propagate through a region. Unlike eddy transport, dynamical transport can occur even in the absence of a concentration gradient. The effects of dynamical transport are usually neglected in chemical models of the middle and upper atmosphere. Our direct measurements of the vertical dynamical flux of Na shows that dynamical transport is at least as important as eddy transport. More significantly, the observed Na flux profile is consistent with theoretical predictions, in the region between 85 and 93 km where the wave dissipation is strong.

In most cases it will not be possible to directly measure constituent fluxes since simultaneous common volume profiles of vertical wind and constituent densities are required. Fortunately, our results suggest that the dynamical flux can be modeled using Eq. (6) when chemical effects can be neglected. The constituent fluxes can then be predicted using measurements of the vertical heat flux profile. While dissipating gravity waves contribute to both dynamical and eddy transport, our theoretical and observational results show that the dynamical transport is a significant and important transport mechanism in the mesopause region.

Acknowledgements

The authors gratefully acknowledge Xinzhao Chu and Peter Dragic for their help in acquiring the SOR lidar observations. We also thank Robert Fugate, Director of the Starfire Optical Range, and his staff for allowing us to use this impressive facility and for their help with the installation and operation of the Illinois lidar. This work was supported by NSF grants ATM 94-03036 and ATM 97-09921.

Appendix: Statistics of the Na number density perturbations

The unperturbed Na layer can be accurately modeled by a Gaussian distribution (Senft and Gardner, 1991)

$$\bar{\rho}_{\mathrm{Na}}(z) = \frac{A_{\mathrm{Na}}}{\sqrt{2\pi}\sigma_{\mathrm{Na}}} \exp\left[-\frac{(z - z_{\mathrm{Na}})^2}{2\sigma_{\mathrm{Na}}^2}\right], \quad (A.1)$$

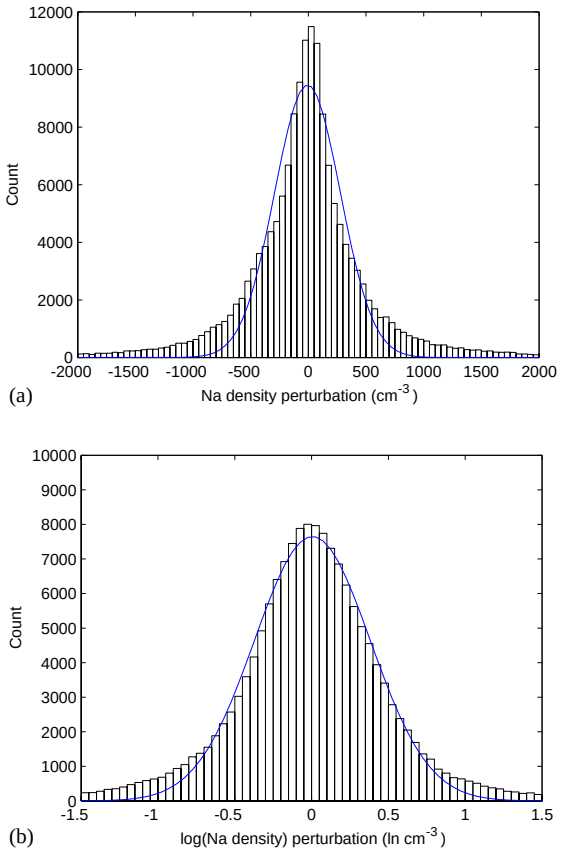

Fig. 5. Histograms of (a) Na number density perturbations and (b) log Na number density perturbations. The solid lines are their Gaussian fits.

where A_{Na} is the Na abundance ($\sim 5\times10^{-9}/\mathrm{cm}^2$), z_{Na} is the layer centroid height (~ 92 km), and $\sigma_{Na}(\sim 4.5$ km) is the rms layer thickness. The perturbed number density profile is obtained by substituting Eq. (A.1) in Eq. (4).

$$\rho_{Na}(z)=\bar{\rho}_{Na}(z)\exp\left\{\frac{1}{(\gamma-1)}\left[1-\frac{\gamma H}{\sigma_{Na}^2}(z-z_{Na})\right]\frac{T'}{\bar{T}}\right.$$

$$\left.-\frac{1}{2}\left[\frac{\gamma H}{(\gamma-1)\sigma_{Na}}\right]^2\left(\frac{T'}{\bar{T}}\right)^2\right\}. \qquad (A.2)$$

Because the rms relative temperature perturbations are less than 5%, the term involving $(T'/\bar{T})^2$ is negligible in Eq. (A.2). Because T' is Gaussian distributed, the distribution of the Na number density is approximately log-normal. Plotted in Fig. 5 are histograms of the fluctuations of the Na number density and the logarithm of the Na number density along with the best-fit Gaussian distributions. As predicted the log-normal distribution provides a better fit to the data than a Gaussian distribution. However, the differences are not great. For the purposes of estimating the Na flux measurement errors, we employ the simpler Gaussian model.

References

Bills, R.E., Gardner, C.S., 1993. Lidar observations of the mesopause region temperature structure at Urbana. Journal of Geophysical Research 98, 1011–1021.

Colegrove, F.D., Johnson, F.S., Hanson, W.B., 1966. Atmospheric composition in the lower thermosphere. Journal of Geophysical Research 71, 2227–2236.

Franke, S.J., Chu, X., Liu, A.Z., Hocking, W.K., 2004. Comparison of meteor radar and Na doppler lidar measurements of winds in the mesopause region above Maui, HI. J. Geophys. Res., submitted.

Fritts, D.C., Dunkerton, T.J., 1985. Fluxes of heat and constituents due to convectively unstable gravity waves. Journal of Atmospheric Science 42, 549–556.

Fritts, D.C., van Zandt, T., 1993. Spectral estimates of gravity wave energy and momentum fluxes: Part I: Energy dissipation, acceleration, and constraints. Journal of Atmospheric Science 50, 3685–3694.

Garcia, R.R., Solomon, S., 1985. The effect of breaking gravity waves on the dynamics and chemical composition of the mesosphere and lower thermosphere. Journal of Geophysical Research 90, 3850–3868.

Gardner, C.S., Shelton, J.D., 1985. Density response of neutral atmospheric layers to gravity wave perturbations. Journal of Geophysical Research 90, 1745–1754.

Gardner, C.S., Yang, W., 1998. Measurements of the dynamical cooling rate associated with the vertical transport of heat by dissipating gravity waves in the mesopause region at Starfire Optical Range, New Mexico. Journal of Geophysical Research 103, 16909–16926.

Gardner, C.S., Franke, S.F., Yang, W., Tao, X., Yu, J.R., 1998. Interpretation of gravity waves observed in the mesopause region at Starfire Optical Range, New Mexico: Strong evidence for nonseparable intrinsic (m,ω) spectra. Journal of Geophysical Research 103, 8699–8713.

Gardner, C.S., Gulati, K., Zhao, Y., Swenson, G., 1999. Measuring gravity wave momentum fluxes with airglow imagers. Journal of Geophysical Research 104, 11903–11915.

Gardner, C.S., Zhao, Y., Liu, A.Z., 2002. Atmospheric stability and gravity wave dissipation in the mesopause region. Journal of Atmospheric, Solar and Terrestrial Physics 64, 923–929.

Grime, B.W., Kane, T.J., Liu, A.Z., Papen, G., Gardner, C.S., Kelley, M.C., Kruschwitz, C., Drummond, J., 2000. Meteor trail advection observed during the 1998 Leonid shower. Geophysical Research Letters 27, 1819–1822.

Hickey, M.P., Walterscheid, R.L., Richards, P.G., 2000. Secular variations of atomic oxygen in the mesopause region induced by transient gravity wave packets. Geophysical Research Letters 27 (21), 3599–3602.

Hocking, W.K., 1986. Observation and measurement of turbulence in the middle atmosphere with a VHF radar. Journal of Atmospheric and Terrestrial Physics 48, 655–670.

Hocking, W.K., 1990. Turbulence in the region 80–120 km. Advances in Space Research 10, 153–161.

Hocking, W.K., Walterscheid, R.L., 1993. The role of Stokes' diffusion in middle atmospheric transport. In: Thrane, E.V., Blix, T.A., Fritts, D.C. (Eds.), NATO (North Atlantic Treaty Organization) Publication in Coupling Process in the Lower and Middle Atmosphere, Series C: Mathematical and Physical Sciences, Vol. 387, Kluwer Academic Publishers, Dordrecht, Boston and London, pp. 305–328.

Hodges Jr., R.R., 1967. Generation of turbulence in the upper atmosphere by internal gravity waves. Journal of Geophysical Research 72, 3455–3458.

Kudeki, E., Franke, S.J., 1998. Statistics of momentum flux estimation. Journal of Atmospheric, Solar and Terrestrial Physics 60, 1549–1553.

Larsen, M., Liu, A.Z., Bishop, R.L., Hecht, J.H., 2003. TOMEX: a comparison of lidar and sounding rocket chemical tracer wind measurement. Geophysical Research Letters 39 (7), 1375.

Lindzen, R.S., 1981. Turbulence and stress owing to gravity wave and tidal breakdown. Journal of Geophysical Research 86, 9707–9714.

Liu, A.Z., Hocking, W.K., Franke, S.J., Thayaparan, T., 2002. Comparison of Na lidar and meteor radar wind measurements at Starfire Optical Range, NM, USA. Journal of Atmospheric, Solar and Terrestrial Physics 64, 31–40.

Lübken, F.J., 1997. Seasonal variation of turbulent energy dissipation rates at high latitudes as determined by in situ measurements of neutral density fluctuations. Journal of Geophysical Research 102, 13441–13456.

Lübken, F.J., Hillert, W., Lehmacher, G., von Zahn, U., 1993. Experiments revealing small impact of turbulence on the energy budget of the mesosphere and lower thermosphere. Journal of Geophysical Research 98, 20369–20384.

Lübken, F.J., Hillert, W., Lehmacher, G., von Zahn, U., Blix, T.A., Thrane, E.V., Widdel, H.U., Kokin, G.A., Knyazev, A.K., 1994. Morphology and sources of turbulence in the mesosphere during DYANA. Journal of Atmospheric and Terrestrial Physics 56, 1809–1833.

Mengel, J.G., Mayr, H.G., Chan, K.L., Hines, C.O., Reddy, C.A., Arnold, N.F., Porter, H.S., 1995. Equatorial oscillations in the middle atmosphere generated by small scale gravity waves. Geophysical Research Letters 22, 3027–3030.

Mlynczak, M.G., Solomon, S., 1993. A detailed evaluation of the heating efficiency in the middle atmosphere. Journal of Geophysical Research 98, 10517–10541.

Papen, G.C., Gardner, C.S., Pfenninger, W.M., 1995. Analysis of a potassium lidar system for upper-atmospheric wind-temperature measurements. Applied Optics 34, 6950–6958.

Plane, J.M.C., Gardner, C.S., Yu, J., She, C.Y., Garcia, R.R., Pumphrey, H.C., 1999. Mesospheric Na layer at 40°N: modeling and observations. Journal of Geophysical Research 104, 3773–3788.

Reid, I.M., Vincent, R.A., 1987. Measurements of mesospheric gravity wave momentum fluxes and mean flow accelerations at Adelaide, Australia. Journal of Atmospheric and Terrestrial Physics 49, 443–460.

Riese, M., Offerman, D., Brasseur, G., 1994. Energy released by recombination of atomic oxygen and related species at mesopause heights. Journal of Geophysical Research 99, 14585–14593.

Senft, D.C., Gardner, C.S., 1991. Seasonal variability of gravity wave activity and spectra in the mesopause region at Urbana. Journal of Geophysical Research 96, 17229–17264.

Tao, X., Gardner, C.S., 1995. Heat Flux observations in the mesopause region above Haleakala. Geophysical Research Letters 22, 2829–2832.

Thrane, E.V., Blix, T.A., Hall, C., Hansen, T.L., von Zahn, U., Meyer, W., Czechowsky, P., Schmidt, G., Widdel, H.U., 1987. Small scale structure and turbulence in the mesosphere and lower thermosphere at high latitudes in winter. Journal of Atmospheric and Terrestrial Physics 49, 751–762.

Tsuda, T., Murayama, Y., Yamamoto, M., Kato, S., Fudao, S., 1990. Seasonal variation of momentum flux in the mesosphere observed with the MU radar. Geophysical Research Letters 17, 725–728.

Walterscheid, R.L., 1981. Dynamical cooling induced by dissipating internal gravity waves. Geophysical Research Letters 8, 1235–1238.

Walterscheid, R.L., 2001. Gravity wave transports and their effects on the large-scale circulation of the upper mesosphere and lower thermosphere. Advances in Space Research 27, 1713–1721.

Walterscheid, R.L., Hocking, W.K., 1991. Stokes diffusion by atmospheric internal gravity waves. Journal of Atmospheric Science 48, 2213–2230.

Walterscheid, R.L., Schubert, G., 1989. Gravity wave fluxes of O_3 and OH at the nightside mesopause. Geophysical Research Letters 16, 719–722.

Walterscheid, R.L., Schubert, G., Straus, J.M., 1987. A dynamical-chemical model of wave driven fluctuations in the OH nightglow. Journal of Geophysical Research 92, 1241–1254.

Watkins, B.J., Philbrick, C.R., Balsley, B.B., 1988. Turbulence energy dissipation rates and inner scale sizes from rocket and radar data. Journal of Geophysical Research 93, 7009–7014.

Weinstock, J., 1984. Gravity wave saturation and eddy diffusion in the middle atmosphere. Journal of Atmospheric and Terrestrial Physics 46, 1069–1082.